7.6 EVALUATION OF REMOTE ICING DETECTION TECHNIQUES USING X-, K_a-, AND W-BAND RADAR AND MICROWAVE RADIOMETER OBSERVATIONS

John K. Williams*, J. Vivekanandan and Guifu Zhang
National Center for Atmospheric Research, Boulder, Colorado

1. INTRODUCTION

Reliable remote sensing of super-cooled liquid water could improve aviation safety in winter weather by enhancing the detection of aircraft icing conditions. Previous studies have suggested the potential of techniques using reflectivity differences from dual-wavelength radars, or single wavelength measurements along with a radiometer-derived integrated water path, to accurately retrieve range-resolved liquid water content in clouds. Under the auspices of the FAA's Aviation Weather Research Program, NCAR is evaluating these techniques with a view toward developing an integrated fuzzy-logic algorithm for producing dependable profiles of cloud liquid water content and droplet size.

Two recent field programs, the Mount Washington Icing Sensor Project (MWISP) and the Alliance Icing Research Study (AIRS), supplied X-, K_a-, and W-band polarized Doppler radar data and coordinated radiometer measurements that may be used to compare three promising retrieval methods. Results are presented below for a case from MWISP in which data for all three bands are available, and the potential for integrating these methods into a combined technique is discussed.

2. RETRIEVAL METHODS

Three promising methods for retrieving cloud liquid water content (LWC) profiles from radar and radiometer measurements are described below.

2.1 *Method 1: Dual-wavelength reflectivities*

The dual-wavelength method is based on the observation that liquid water attenuates radar signals differently depending on their wavelengths (Doviak and Zrnić, 1993; Vivekanandan, et al., 1999 and 2001). At radar wavelengths, attenuation due to small-droplet scattering is relatively insignificant. Therefore, the measured reflectivity at a range h from a radar having wavelength λ, $Z_\lambda(h)$, depends on the reflectivity in the radar sampling volume, $Z(h)$, and the two-way absorption of the intervening medium:

$$Z_\lambda(h) = Z(h)e^{-2\int_0^h \sigma_{abs}(\lambda,z)dz}. \tag{1}$$

Taking $10\log_{10}$ and the derivative of both sides, it follows that

$$\frac{\partial}{\partial h}\left(dBZ_{\lambda_1}(h) - dBZ_{\lambda_2}(h)\right) = 20\log_{10}(e)\left(\sigma_{abs}(\lambda_2,h) - \sigma_{abs}(\lambda_1,h)\right). \tag{2}$$

If the attenuation due to water vapor and oxygen is relatively small or the measured dBZ difference has been adjusted for it, then $\sigma_{abs} \approx \sigma_{liq}$, the absorption due to liquid water. When the water droplets are sufficiently small to be approximately spherical and are much smaller than λ, Mie theory may be used to write

$$\sigma_{liq}(\lambda,h) = \frac{6\pi}{\rho_w \lambda} L(h)\,\mathrm{Im}[-K(\lambda,T(h))] \tag{3}$$

(Doviak and Zrnić, 1993). Here ρ_w is the density of water, $L(h)$ is the liquid water content in the same units, λ has the same units as h, and $K = (m^2-1)/(m^2+2)$; the complex index of refraction of water, m, is a function of the wavelength and temperature. With these substitutions, equation (2) relates $L(h)$ to the range derivative of the radar dBZ difference at h. In practice, radar measurements are available only at discrete range gates, so sums are used in place of the integrals above and the derivative is estimated using a finite difference over range. Noise in the measurements or the presence of large droplets may require that the $dBZ_{\lambda_1} - dBZ_{\lambda_2}$ difference profiles first be fit by a monotone increasing function.

Once a liquid water profile has been computed and Z has been estimated by inverting equation (1), a useful estimate of particle diameter, called radar estimated size (RES), may be obtained from

$$\mathrm{RES} = \left(\frac{\langle D^6\rangle}{\langle D^3\rangle}\right)^{1/3} = \left(\frac{\pi\rho_w}{6}\frac{Z}{L}\right)^{1/3} \tag{4}$$

(Vivekanandan, et al., 2001), where $\langle D^n\rangle$ denotes the n^{th} moment of the droplet size distribution and ρ_w the density of water.

2.2 *Method 2: Gamma distribution fit*

Empirical data suggest that cloud water droplet sizes may be well-approximated by the normalized Gamma distribution,

$$N(D) = N_t \frac{\Lambda^{\mu+1} D^\mu e^{-\Lambda D}}{\Gamma(\mu+1)}, \tag{5}$$

where N_t denotes the total droplet number density, D is the droplet diameter, and Γ is the Euler gamma function. If the size distribution parameters μ and Λ are known, the cloud liquid water content and reflectivity may be obtained from the third and sixth moments, respectively:

$$L = \frac{1}{6}\pi\rho_w\langle D^3\rangle = \frac{1}{6}\pi\rho_w N_t \frac{(\mu+3)(\mu+2)(\mu+1)}{\Lambda^3} \tag{6}$$

and

$$Z = \langle D^6\rangle = N_t \frac{(\mu+6)\cdots(\mu+2)(\mu+1)}{\Lambda^6}. \tag{7}$$

The units of ρ_w, N_t, and Λ are generally chosen so that L has units of g/m^3 and Z has units mm^6/m^3.

* *Corresponding author address:* John K. Williams, National Center for Atmospheric Research, P.O. Box 3000, Boulder, CO 80307; email: jkwillia@ucar.edu.

Using radar-measured reflectivities dBZ_1', …, dBZ_n' at n range gates and the total integrated water path, L_{tot}, obtained from a radiometer or sounding, it is possible to fit $n+1$ free parameters of the droplet distributions over those ranges. The droplet number density, N_t, has been found to be roughly constant throughout stratus clouds (Frisch, et al., 1995), and setting $\mu = 1$ still allows a reasonable collection of candidate distribution functions, as illustrated in Figure 1. Given any choice of N_t and Λ_1, …, Λ_n, the range-integral of the liquid water contents from (6) and reflectivities obtained via equations (7) and (1) may be compared with the observed L_{tot} and dBZ_1', …, dBZ_n'. Choosing parameter values to minimize the squared error yields a "best-fit" liquid water profile. Other drop size distributions could also be used with this method; e.g., Austin, et al., 2001, used a lognormal distribution and visible optical depth in place of the Gamma distribution and integrated liquid path.

Once they are obtained, the best-fit parameters may be used to produce estimates of the droplet mean diameter, $(\mu+1)/\Lambda$, median volume diameter (MVD), $(\mu+3.67)/\Lambda$, and RES, $[(\mu+6)(\mu+5)(\mu+4)]^{1/3}/\Lambda$.

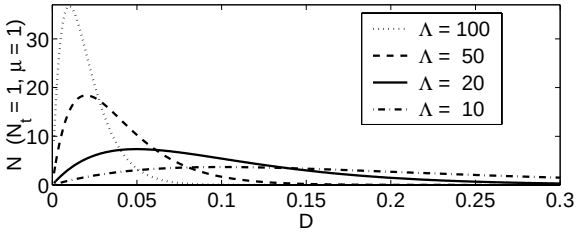

Figure 1: The family of normalized Gamma droplet size distributions from which the best fit is estimated in Method 2. N_t is constant for the profile, Λ varies by range gate, and $\mu = 1$ is fixed. Droplet diameters D may be measured in mm, in which case Λ has units mm^{-1}.

2.3 *Method 3: $Z^{1/2}$ proportional assignment*

A second method for using dBZ_1', …, dBZ_n' and L_{tot} to derive range-resolved liquid water content simply distributes the total water proportionally to the square root of the reflectivities, $Z_k^{1/2}$:

$$L_k = L_{tot} \frac{Z_k^{1/2}}{\sum_{j=1}^{n} Z_j^{1/2} \Delta h_j}, \qquad (8)$$

where Δh_j is the j^{th} range gate spacing. This approach is justified by empirical measurements (Frisch, et al., 1995 and 2000). It is accurate when $\langle D^6 \rangle \propto \langle D^3 \rangle^2$, i.e., $Z \propto L^2$, with the same constant of proportionality for the entire profile. This condition is met when the drop size distribution "shape" and total number density are identical for all ranges. For the Gamma distribution described in Section 2.2, this occurs when

$$\frac{\langle D^6 \rangle}{\langle D^3 \rangle^2} = \left(\frac{\pi \rho_w}{6} \right)^2 \frac{Z}{L^2} = \frac{1}{N_t} \frac{(\mu+6)(\mu+5)(\mu+4)}{(\mu+3)(\mu+2)(\mu+1)} \qquad (9)$$

is constant over range, but this condition is precisely equivalent to the assumption that N_t and μ are fixed for each profile. In general, the relationship between Z and L^2 is quite complex, as illustrated in Figure 2; whether $Z \propto L^2$ for a profile depends on the spatial correlation present under the given meteorological conditions.

In implementing Method 3, the reflectivities, Z_k, must be obtained from the radar-measured Z_k' via equation (1), but this requires that the values of σ_{abs}, and hence L, at gates $1, \ldots, k-1$ already be known. Fortunately, choosing a reasonable starting liquid water profile to obtain absorption coefficient estimates and then iterating the method converges quite rapidly.

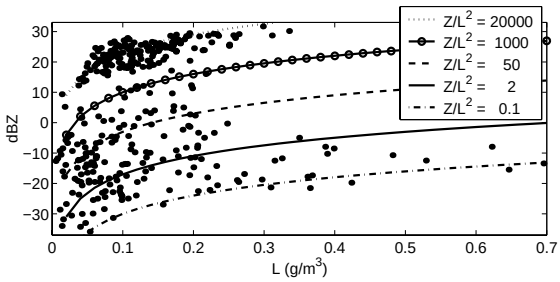

Figure 2: Pairs of liquid content and dBZ values obtained from airborne disdrometer data under no-ice conditions with superimposed constant Z/L^2 curves. The data were collected near Cleveland, OH by the NASA GRC Twin Otter as part of the Supercooled Large Drop Research Program (SLDRP) in February, 1998.

3. COMBINED TECHNIQUE

Synthesizing the three methods described above into a combined technique offers the possibility of producing even more reliable LWC and droplet size profiles. This synthesis could be accomplished using a fuzzy-logic approach: performing quality control on the raw data (e.g., using the Doppler moments and linear depolarization ratio), supplying "confidence" weights for data and for the output of each processing step, and computing a weighted combination of the three methods as the final output. If it is well-designed, such a technique should be more accurate and robust than any retrieval method alone, since each one works well under somewhat different conditions. For instance, Method 1 should give good results when the radar beam widths and sensitivities are well-matched and little Mie scattering is present, and it does not require radiometer data. Method 2 is appropriate when the droplet sizes are well-described by the family of distribution functions being used in the fit, and it supplies output even when only one radar is providing reliable data. Method 3 applies when Z/L^2 is approximately constant throughout the profile, and it can be shown to be insensitive to systematic biases in measured reflectivity values. In fact, output from some methods might be used to censor that from others, yielding additional control over output quality.

The present study is directed at qualitatively assessing the three retrieval methods in order to gauge their potential as part of a combined technique. In future efforts, comparisons of retrievals with in-situ water content and droplet size data from MWISP and AIRS will be used to perform a quantitative evaluation of a combined technique's skill.

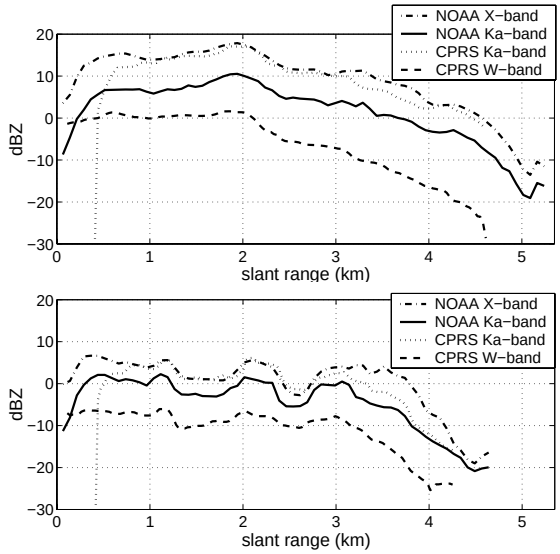

Figure 3: Reflectivities recorded by the NOAA X- and K_a-band radars and the CPRS K_a- and W-band radars at 16:35 (top) and 16:55 UTC (bottom) on April 14, 1999.

4. RESULTS

Both the MWISP and AIRS datsets include coordinated microwave radiometer and X-, K_a-, and W-band polarized Doppler radar measurements suitable for testing the three LWC retrieval methods described above. In MWISP, the NOAA Environmental Technology Laboratory's 3-channel radiometer, NOAA/ETL X- and K_a-band radar, and University of Massachusetts Cloud Profiling Radar System (CPRS) K_a- and W-band radars were used. AIRS employed the Radiometrics 2-channel WVR-1100 radiometer, McMaster University's IPIX X-band radar, and the UMASS CPRS K_a- and W-band radars. In both datasets, the radars provide Doppler moments, reflectivity, and linear depolarization ratio, while the radiometers provide total-path vapor and liquid water measurements.

In this section, results obtained from the three methods using data collected between 16:35 and 17:05 UTC on April 14, 1999, during MWISP are presented. This case was selected because the NOAA X- and K_a-band radars, CPRS K_a- and W-band radars, and NOAA radiometer were all operating and were directed at a common elevation angle of about 20°. In addition, the K_a-band linear depolarization ratios suggest that very little ice or mixed-phase was present.

4.1 Data pre-processing

For each pair of radars, the radar data were pre-processed by interpolating onto the finer of the two range-time grids and applying a 10-second x 150 m median filter; cross-correlations in range and time were computed to ensure that the data were properly aligned. The "cloud top" was identified as the last range gate after at least 250 m of "good" (> –30 dBZ) reflectivity data recorded for both wavelengths. The filtered dBZ values were corrected for attenuation due to atmospheric vapor, oxygen, and nitrogen; to accomplish this, the vapor profile and the attenuation coefficients for the four radar frequencies were computed based on temperature, pressure, and relative humidity profiles recorded by an ATEK sounding taken at 16:22 UTC. In addition, before applying Method 1, the reflectivity differences were adjusted by –5 dB for the CPRS radars and –1 dB for the NOAA radars to account for apparent calibration differences.

Figure 3 shows the reflectivities recorded by the four radars at two times, 16:35 and 16:55 UTC, at ranges up to the cloud top. Median filtering has been performed, but not adjustment for attenuation due to gases or for calibration differences. At 16:55 UTC, clutter from Mt. Washington is evident between about 3 and 4 km; it is most severe for the X-band radar, which has the widest beam (0.9°, as opposed to 0.5° for both K_a-band radars and 0.18° for the W-band radar).

4.2 Method 1 results

Figure 4 displays a comparison between the total integrated water path obtained via Method 1 from the CPRS and NOAA radars with that recorded by the NOAA radiometer between 16:35 and 17:05 UTC. The over-estimate in the CPRS retrieval at the beginning of the time period may be due the presence of large droplets, causing Mie scattering, or to noise. The later underestimate by the CPRS retrieval is probably due to the weakening of the cloud, under which the weak W-band sensitivity only allows a limited portion of the cloud to be measured. The overestimate in the NOAA retrieval after 17:00 UTC is likely due to the strong clutter in the X-band return.

Because of the mismatch in radar beam widths and sensitivities, and the occasional presence of Mie scattering conditions, the reflectivity difference for each pair of radars does not always increase with range, requiring that it be fit by a monotone function before Method 1 is applied. The development of a robust scheme for doing this using image-processing techniques in the space and time domains is still underway; therefore, range-resolved retrievals are not shown here.

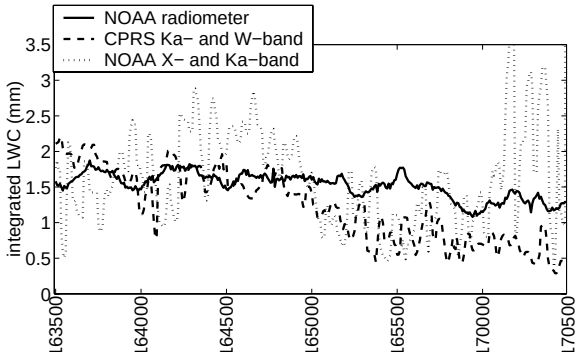

Figure 4: Total liquid path recorded between 16:35 and 16:55 UTC on April 14, 1999, by the NOAA radiometer, with superimposed Method 1 integrated-path retrievals from the CPRS K_a- and W-band (–5 dB adjustment) and the NOAA X- and K_a-band radars (–1 dB adjustment). All instruments were directed at ~20° elevation.

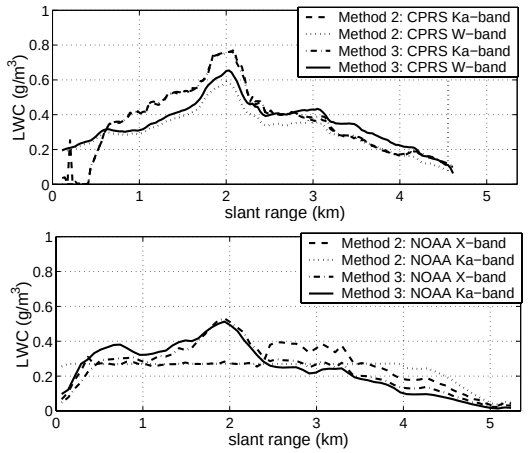

Figure 5: Retrieved liquid water profiles for 16:35 UTC on April 14, 1999, via methods 2 and 3 using the CPRS radars (top) and NOAA radars (bottom).

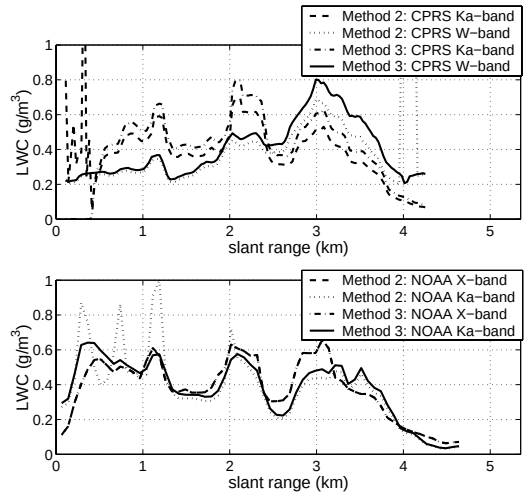

Figure 6: Retrieved liquid water profiles for 16:55 UTC on April 14, 1999, via methods 2 and 3 using the CPRS radars (top) and NOAA radars (bottom).

4.3 Method 2 and 3 results

LWC profiles computed via methods 2 and 3 for all four radars at times 16:35 and 16:55 UTC are shown in Figures 5 and 6, respectively. The Method 2 iteration was halted early; when allowed to converge, its retrievals are identical to those of Method 3. The profiles for 16:35 UTC, where the signal-to-noise ratios are high, exhibit fairly little apparent noise. On the other hand, the returns for 16:55 exhibit suspicious variations, consistent with the presence of clutter and the lower SNR as the cloud dissipates. At both times, values from the CPRS radars are generally higher than those from the NOAA radars. This is due to the fact that the CPRS W-band radar has relatively low sensitivity, so both methods distribute the radiometer-measured total liquid over a smaller range. Nevertheless, the results suggest that, with improved quality control and appropriate confidence weighting, a combined technique based on these three methods should be feasible.

5. CONCLUSION

The three methods presented in this paper show good promise in retrieving reliable liquid water content profiles using coordinated dual-wavelength radar and radiometer data. Furthermore, a combined technique that synthesizes the three methods using a fuzzy-logic approach has the potential to be even more accurate and robust. Such an algorithm will perform data quality control and will assign confidence weights based on the raw data, intermediate processing, and comparisons of the methods' outputs. These values will be used throughout the algorithm and in the final synthesis of the results. In addition, output liquid water and droplet size profiles will be supplied with confidence values, thereby allowing their diagnostic value to be judged.

In future work, a combined algorithm will be developed and evaluated using a number of additional cases from both MWISP and AIRS. Ultimately, a quantitative evaluation will be performed using in-situ data collected from aircraft and ground stations. It is hoped that the combined technique will eventually become part of a practical remote-sensing solution for detecting aircraft icing conditions.

5. ACKNOWLEDGEMENT

This research is in response to requirements and funding by the Federal Aviation Administration (FAA). The views expressed are those of the authors and do not necessarily represent the official policy or position of the FAA.

6. REFERENCES

Austin, R. T., and Stephens, G. L., 2001: Retrieval of stratus cloud microphysical parameters using millimeter-wave radar and visible optical depth in preparation for CloudSat. *J. Geophys. Res.*, 106, 28,233–28,242.

Doviak, R. J., and Zrnić, D. S., 1993: *Doppler Radar and Weather Observations*. Academic Press, 562 pp.

Frisch, A. S., Fairall, C. W., and Snider, J.B., 1995: Measurement of stratus cloud and drizzle parameters in ASTEX with a K_α-band Doppler radar and a microwave radiometer. *J. Atmos. Sci.*, 52, 2788–2799.

Frisch, A. S., Martner, B. E., Djalalova, I., and Poellot, M. R., 2000: Comparison of radar/radiometer retrievals of stratus cloud liquid-water content profiles with in situ measurements by aircraft. *J. Geophys. Res.*, 105, 15,361–15,364.

Vivekanandan, J., Martner, B. E., Politovich, M. K., and Zhang, G., 1999: Retrieval of atmospheric liquid and ice characteristics using dual-wavelength radar observations. *IEEE Trans. on Geosci. Remote Sens.*, 37, 2325–2334.

Vivekanandan, J., Zhang, G., and Politovich, M. K., 2001: An assessment of droplet size and liquid water content derived from dual-wavelength radar measurements on the application of aircraft icing detection. *J. Atm. and Oceanic Tech.*, 18, 1787–1798.